

1 Fragmented Spatial Maps from Surprisal: 2 State Abstraction and Efficient Planning

3 Mirko Klukas^{1*}, Sugandha Sharma¹, YiLun Du², Tomas
4 Lozano-Perez², Leslie Kaelbling², and Ila Fiete^{1*}

5 ¹BCS & McGovern Institute, MIT, Cambridge MA 02139, USA

6 ²EECS & CSAIL, MIT, Cambridge MA 02139, USA

7 *{mklukas, fiete}@mit.edu

8 When animals explore spatial environments, their representations often
9 fragment into multiple maps. What determines these map fragmentations,
10 and can we predict where they will occur with simple principles? We pose
11 the problem of fragmentation of an environment as one of (online) spatial
12 clustering. Taking inspiration from the notion of a *contiguous region* in
13 robotics, we develop a theory in which fragmentation decisions are driven
14 by surprisal. When this criterion is implemented with boundary, grid, and
15 place cells in various environments, it produces map fragmentations from
16 the first exploration of each space. Augmented with a long-term spatial
17 memory and a rule similar to the distance-dependent Chinese Restaurant
18 Process for selecting among relevant memories, the theory predicts the reuse
19 of map fragments in environments with repeating substructures. Our model
20 provides a simple rule for generating spatial state abstractions and predicts
21 map fragmentations observed in electrophysiological recordings. It further
22 predicts that there should be “fragmentation decision” or “fracture” cells,
23 which in multicompartment environments could be called “doorway” cells.
24 Finally, we show that the resulting abstractions can lead to large (orders
25 of magnitude) improvements in the ability to plan and navigate through
26 complex environments.

27 Introduction

28 Contextual reorientation [1], in which behavior, state estimates, or meaning are suddenly
29 reevaluated and reanchored based on new or altered contextual information from the
30 world, are universal phenomena in psychology. One interesting set of examples is the
31 parsing of garden-path sentences such as “Time flies like an arrow, fruit flies like a

32 banana” or “The woman brought the sandwich from the kitchen tripped” [2]. In the
 33 latter there is a sudden reorientation upon hearing the word tripped, so that *the woman*
 34 becomes the person *who was* brought the sandwich rather than the person bringing the
 35 sandwich. Similarly, spatial reorientation and reanchoring can occur when entering a
 36 building lobby from the outside or entering a different looking room from another one.
 37 Such reanchoring or reorientation events may constitute the basis on which we segment
 38 the continuous stream of experience into episodes or chunks to structure experience and
 39 memory [3–5].

40 In the brain, grid cells construct continuous 2-dimensional Euclidean maps of small en-
 41 vironments [6] by the integration of self-movement cues as the animal explores the space,
 42 Fig. 1a. The advantage of such velocity integration-based Euclidean representations is
 43 that they provide a consistent encoding of seen and unseen locations and independent
 44 of paths taken to get there, making it possible to compute novel shortcut paths and
 45 perform spatial inference between locations [7–12].

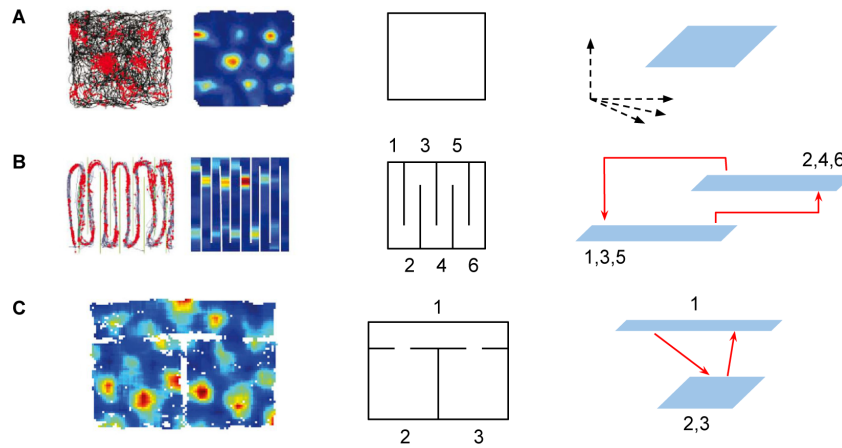


Figure 1: Map fragmentation in MEC. **A-C: Left, Middle:** Firing fields of grid cells in various environments (firing fields in A,B from [13] and in C from [14]). Environments are illustrated schematically in the middle column (open field, hairpin, and two-room with hallway). **Right:** Schematic map fragmentations of the environments. Blue regions are submaps, or regions with a continuous representation in the state space of the multi-module grid cell population. Solid arrows indicate discontinuous jumps in grid phase, which we interpret as transitions between submaps.

46 However, in more complex spaces with compartments or subregions [13, 14], Fig. 1b-
 47 c, the grid cell spatial representation is often not a globally consistent 2-dimensional
 48 map that can be predicted by path integration even when the agent moves smoothly
 49 and continuously across the space. Instead, the neural representations exhibit a frac-
 50 tured structure across the space, referred to in the literature as map fragmentation.
 51 We hypothesize a direct connection between cognitive reanchoring and the formation of
 52 fragmented spatial maps including the general phenomenon of remapping.

53 It is well known that between different environments, place and grid cells “remap”:

54 Representations of different environments involve different (if overlapping) sets of place
55 cells and the spatial relationships between place cells in one environment are not pre-
56 served in the other [15]. Grid remapping is seemingly more subtle, but consistent with
57 place cell remapping: within modules, grid cells maintain their relationships and thus
58 shift their phases coherently, but across modules, there are differential or incoherent
59 shifts in phase [16]. Remapping is typically studied by discontinuously transplanting
60 subjects from one environment to another or by switching non-spatial cues [15, 17]: by
61 inducing large spatial changes through a journey in a closed container or vehicle or cue-
62 less corridor where the subject cannot easily determine its spatial displacement, or by
63 altering olfactory or visual cues within the same space. Map fragmentation – because
64 it involves the continuous movement of an agent through a stationary environment – is
65 viewed differently from remapping, in which the emphasis is on an externally-induced envi-
66 ronmental change [15, 18]. However, map fragmentation should be viewed as remapping
67 or reanchoring within an environment; here we seek to provide a unified model of map
68 fragmentation and explore its potential utility.

69 A cost of map fragmentation is the loss of the ability to perform path-integration based
70 computations across the environment [7–11]. We hypothesize that map fragmentation
71 is a solution to multiple problems: First, it solves the problem of the accumulation of
72 path integration errors that prevent the formation of consistent maps over larger spaces,
73 resulting in the formation of smaller but consistent Euclidean maps. Thus, map frag-
74 mentation enables spatial inference and shortcut behaviors within each submap. Second,
75 each submap represents a state abstraction in which contiguous locations are clustered
76 together, and combining these abstractions with links between them can permit effi-
77 cient and hierarchical representation and planning. Third, submaps can combine more
78 globally to form a “topometric” map, a representation with enough expressiveness for
79 topologically non-trivial cognitive spaces beyond real space, that preserves the advan-
80 tages of both local metric structure and global hierarchy and abstraction.

81 Here, we propose a simple online rule for map fragmentation that avoids the large
82 memory, time complexity and data-inefficiency of offline algorithms, and show that the
83 resulting rule is a good potential model of map segmentations observed in grid and place
84 cells. Finally, we demonstrate by implementing efficient random tree search algorithms
85 that map fragmentation can facilitate efficient planning relative to using global maps,
86 leading to a massive speed-up in complex and large environments without repeated
87 substructures.

88 **Results**

89 **Map fragmentation as clustering: an offline baseline**

90 We propose that remapping across environments and fragmentation within environments
91 can be considered to be a clustering problem: At each sampled location, the question is
92 whether it should be categorized as a part of the most recently used map, or be assigned
93 to a different one. A sensible answer would be that sufficiently “similar” locations should
94 be assigned to the same map (cluster), while sufficiently different ones should be assigned

95 to different maps (clusters).

96 We view a map as a (local) world model that enables the prediction of sensory inputs
97 at any location within the map. Thus, we consider that a key metric for map frag-
98 mentation may be predictability or surprisal, Fig. 2. A similar metric has been used
99 in robotics methods for simultaneous localization and mapping (SLAM) [19]. Specif-
100 ically, sets of poses (locations and orientations) where the predictability of external
101 observations remains high while moving between them (“contiguous regions”) should be
102 clustered together into one map, Fig. 2. This view complements the use of other metrics
103 that have been implemented in offline settings to construct spatial maps, including the
104 graph Laplacian [20] and successor representation [21] methods, both of which use tem-
105 poral proximity as their metric (indeed, under a random exploration policy, the successor
106 representation is closely related to the graph Laplacian). Our primary focus here is on
107 how biological and artificial agents might generate sensible maps in an online fashion.
108 Secondly, we use the metric of prediction or surprisal to generate these online frag-
109 mentations. In Discussion, we will consider how additional metrics can be used within
110 the same online framework.

111 Define a model $\mathbb{P}(z' | x', x, z)$ that predicts the sensory input z' at pose x' , based
112 on the sensory input z at pose x (Fig. 2a,b; see Methods for details). The sensory
113 observations and their predictions are given in terms of a range sensor centered on the
114 agent, in the actual environment (Fig. 2a, right) or in a reconstructed map based on
115 the observations z (Fig. 2a, middle), respectively. For each pose x , we delineate the
116 surrounding region where predictability remains above threshold; this, by definition, is a
117 contiguous region. We call the boundary of the region the prediction horizon for x . The
118 radius of the prediction horizon varies depending on location within the environment,
119 Fig. 2c. We can use the mutual surprise between poses, which we define as $-\frac{1}{2}(\log \mathbb{P}(z' |$
120 $x', x, z) + \log \mathbb{P}(z | x, x', z'))$ (see Methods for details), as a measure of proximity that
121 we illustrate with an Isomap embedding [22] of the environment (Fig. 2d). In this
122 visualization, contiguous (high predictability) regions are compressed, while transition
123 or bottleneck regions (low predictability) are stretched.

124 Finally, we define the average surprisal (see Methods) of a pose x by averaging over the
125 mutual surprise of all nearby poses at a fixed Euclidean distance, and apply a clustering
126 procedure similar to DBSCAN [23]¹. The procedure computes the connected components
127 of all locations whose average surprise lies below a fixed threshold and decomposes
128 the map into core fragments and transition regions, Fig. 2e. Additionally, in order to
129 make an informed choice about the fragmentation threshold, we compute a contour tree
130 (cf. [24]) of the surprisal values, which provides a visualization of how the connectivity
131 of space evolves with increasing thresholds, Fig. 2f. As we see, there are regions of the
132 contour tree that are relatively robust to the detailed threshold choice, providing similar
133 connectivities over a range of threshold values.

134 The surprisal-based segmentations align well with both intuitive fragmentations and
135 with neural data (cf. Fig. 1), suggesting that predictability may be a key and principled

¹The density notion in DBSCAN is based on a count of neighbors. We use the average mutual surprise instead.

136 objective for map segmentation decisions.

137 However, the algorithm is offline, requiring full exploration of the space before it can
138 generate the fragmented map. This is unlike in experiments, where animals generate
139 map fragmentations in real-time as they explore an environment [14]; in non-spatial
140 contexts too, there is evidence that event boundaries are defined in real-time [5, 25].
141 The algorithm also has high complexity, requiring fine spatial discretization and a large
142 memory and computational buffer for the storage of and computation on the full predic-
143 tivity matrix over all pairs of positions in the space. The same is true for Laplacian and
144 successor matrix-based methods. Further, there is an additional gap between observed
145 map fragmentations in biology and the latter two algorithms because while they provide
146 multi-scale representations of the space (in the form of eigenvectors of some similarity
147 matrix), they are not actually fragmentations of the environment, Fig. S3,S4.

148 **Online fragmentation based on predictability: Our model**

149 We next build a simple and biologically plausible online map fragmentation model based
150 on short-term prediction error as an efficient proxy for surprisal, with the goal of gen-
151 erating fragmentations that are consistent with the principled offline clustering-based
152 algorithm above. Our model is an agent that integrates its velocity as it explores an
153 environment to update its pose estimate, and uses a short-term memory (STM) and a
154 long-term memory (LTM) to make predictions about what it expects to see next.

155 The sensory observations for the online model consist of the activities of a population
156 of cells that encode the presence of environmental boundaries at some distance, similar
157 to boundary vector cells (BVCs) [26, 27] in entorhinal cortex or boundary-coding cells
158 in the occipital place area [28]. These encode a binary, idiothetically-centered local view
159 of the space² (with observation field-of-view angle ϕ), Fig. 3a,c. The velocity-based
160 position estimates are represented by a population of idealized grid cells from multiple
161 modules. For simplicity and to match the experimental setups in [13, 14] we assume that
162 the pose angle is specified by a global orienting cue – effectively, the agent has access to
163 its true head direction. The STM consists of an exponentially decaying moving average
164 of recent observations, each shifted according to the internal velocity estimate of the
165 agent, Fig. 3d. The STM is used to generate the prediction for the next observation
166 (motivated by [19]), and a normalized dot product between the prediction and the cur-
167 rent observation (BVC activity) yields our predictability signal (Fig. 3b,e). Due to its
168 implementation as a moving average, STM activity slightly lags BVC activity. While
169 high predictability is maintained along a trajectory, no fragmentation occurs. Once the
170 predictability signal dips below a threshold, then at the first subsequent stabilization of
171 spatial information, signaled by predictability returning to threshold, a fragmentation
172 event is triggered (Fig. 3b). The fragmentation decision thus segments or chunks the
173 continuous stream of experience based on the content of the experience, with similar
174 observations chunked together and separately from dissimilar ones. It is an event that
175 is discrete in space and time and drives a discrete fracture or fragmentation in the in-

²This is also known as a grid occupancy map in robotics [29].

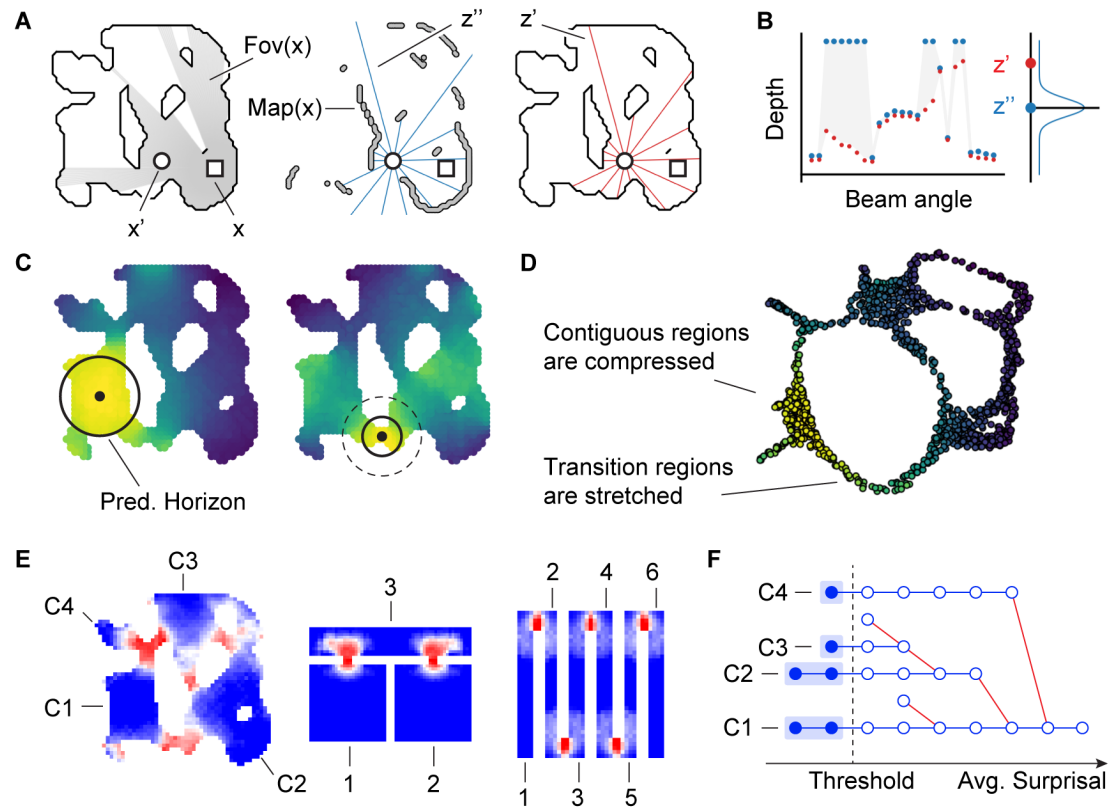


Figure 2: Fragmentations from predictability-based clustering. **A:** *Left.* Two agents (circle and square) in an organically shaped environment, with gray indicating the square agent's field of view. *Middle.* A set of range sensor observations (blue, z'') by the circular agent, shown on the map built from the square-agent's observations. *Right.* A set of range sensor observations (red, z') by the circular agent, shown on the actual environment. **B:** The blue observations in A constitute the square agent's prediction of the circular agent's measurements, with a prediction model given by a multivariate diagonal Gaussian with means given by the blue measurements, and which is evaluated at the vector of actual measurements in red. Greater vertical deviations between red and blue dots correspond to larger prediction errors. **C:** Each black dot represents a fixed reference location. All locations (pixels) in the map are colored by their predictability from the reference location. Solid black circle: the prediction horizon at that reference location: The horizon is large in open (contiguous) spaces, and small at bottleneck (transition) regions. **D:** An Isomap embedding of the environment based on mutual predictability gives rise to a warped embedding: distances are large when predictability is low. **E:** Locations in three environments, colored by their *average surprisal*. Numbered subregions correspond to connected components with average surprisal below a threshold level. **F:** A hierarchical clustering tree for the evolution of connected subregions for the first environment from E: Although the delineation of subregions depends on the choice of threshold, some subregions are relatively persistent and thus robust, maintaining their identity over a range of thresholds.

176 ternal map that translates to a discontinuous jump in the large encoding space of the
 177 multi-periodic grid cell population.

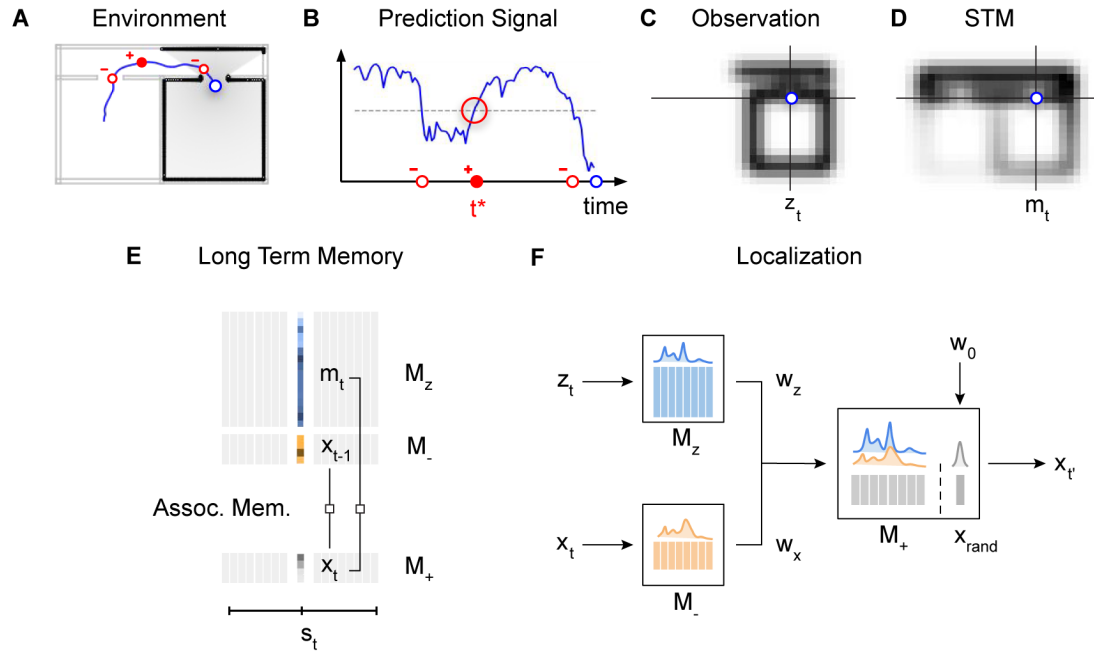


Figure 3: Online fragmentation model. **A:** Sample trajectory (blue) through a “2-room” environment highlighting three distinct events (red circles) that map to the events in B. Gray area: the agent’s field of view at the agent’s current location (blue circle). **B:** Prediction signal for the trajectory in A. Red dots indicate when the prediction crosses a threshold (dashed line), with the filled dot indicating a map fragmentation event (which occur at upward threshold crossings). **C** A snapshot of the current observation (z_t), which here consists of idiomatically centered BVC inputs to the agent (located at blue dot). Each pixel represents a BVC tuned to a location in space specified by the vector displacement between the agent and the pixel. Pixel intensity indicates the level of BVC activation. The image is cropped to exclude inactive BVCs. **D** Activity of the cell population encoding the STM (m_t) of recent observations for the trajectory from A. The STM slightly lags the current observation. Our prediction signal is derived from a normalized dot-product between the current observation and the STM. **E:** At each time t , the model stores associations between the STM m_t , the internal positional code x_t , and its predecessor x_{t-1} in a long-term memory (LTM). The slots s_t in the memory are chosen randomly. **F:** At a fragmentation event, the current observation z_t is compared to the LTM of observations M_z (blue columns), while the current position x_t is compared with the corresponding LTM of predecessor positions M_- . These comparisons result in weights w_z and w_x , respectively, and a memory is probabilistically selected for reuse from the LTM in proportion to its weight. Additionally, with a fixed probability, a random new map is initiated.

178 Once a decision to fragment has been made the agent must make a second decision,
 179 about which map fragment to use next, for which it uses its LTM. The LTM consists of
 180 past associations between the grid cell-encoded position representations and the sensory
 181 observations, filtered through the STM. Thus each LTM entry represents a gist of the
 182 sequence of observation-position pairings over an interval given by the time-constant
 183 of the STM (Fig. 3f). At the fragmentation event, the agent searches the LTM and

184 stochastically selects a state in proportion to its match between items in LTM the current
185 observation-position pairing. With some small constant probability (Fig. 3g), the agent
186 selects (initializes) a new map, which corresponds to selecting a randomized new internal
187 grid-coded position representation by randomizing the set of phases across the grid
188 modules.

189 The stochastic selection of an item from LTM based on overlap with the current
190 observation serves two purposes simultaneously: first, an observation is likely to drive
191 selection of a closely matching prior observation, and second, the retrieval of a previous
192 observation is also proportional to the number of times that observation has been made
193 before, because stochastic selection from the set of past observations is a form of monte
194 carlo volume estimation. In short, the selection of a submap after a fragmentation
195 decision enables the reuse of existing submaps to represent new spaces when relevant
196 based on similarity and frequency of past observations, while simultaneously permitting
197 the creation of new maps. The frequency-dependence of this process together with
198 the possibility to create new maps is similar to the Bayesian nonparametric Chinese
199 Restaurant Process (CRP) [18, 30, 31]; the observational similarity component makes it
200 more akin to the distance dependent CRP (dd-CRP) [32, 33]. However, in contrast with
201 the CRP, observations in the present version of our model are only implicitly clustered
202 into submaps: temporally-averaged observation-location pairs are stored independently
203 of the rest in the LTM without an explicit submap assignment, with submap boundaries
204 defined by the existence of a discrete fragmentation decision and a discontinuous jump
205 in the grid-encoded spatial locations for the post-fragmentation observation relative to
206 the immediate pre-fragmentation observation ³.

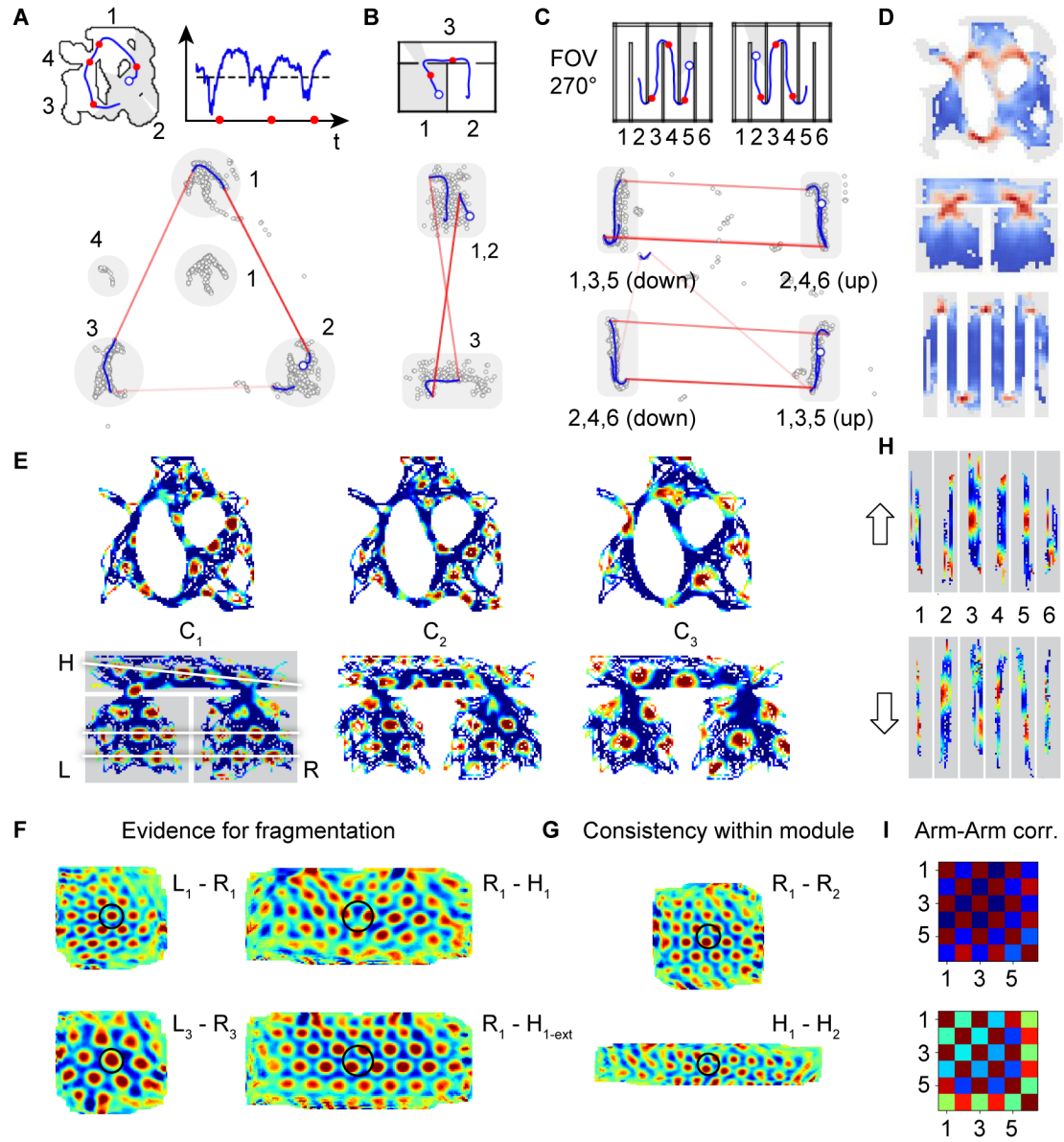
207 Further maintaining a “temporal” LTM which memorizes spatial transition probabil-
208 ities, and using this information to bias the selection of a map at fragmentation events
209 stabilizes how an environment is fragmented, though it is not critical (see SI, Fig. S6).
210 Spatial transitions contain valuable information about the relationships between indi-
211 vidual map fragments and are important for exploiting their hierarchical structure in
212 route planning, as we illustrate later.

213 **Fragmented maps in multiple environments**

214 We explore the map fragmentations generated by our online model across organically
215 shaped and previously experimentally tested structured multi-compartment environ-
216 ments, Fig. 4. The online model generates fragmentations at locations that correspond
217 to observation bottlenecks, including at doorways or narrow openings and around the
218 corner of sharp turns, Fig. 4a-c (top). Starting from the first trajectory through the
219 space and across multiple trajectories, the remapping or fragmentation points and the

³A temperature hyperparameter controls the degree of noise in the selection of a submap from LTM. This stochastic process allows us to not only use the degree of similarity but also the frequency of similar observations in selecting a submap: it performs a stochastic measurement of the volume of similar observations (submap occupancy), and then stochastically selects a map on that basis, without keeping an explicit count of how often each submap has been visited in the past. Thus, we may call this process a doubly-stochastic dd-CRP.

220 selected maps are consistent, evidence of the robustness and reliability of online frag-
221 mentation (Fig. 4a-c, bottom). In the two-room and hallway environment, the model
222 generates a fragmentation in which the two rooms are each represented by the same local
223 map (rather than a single global map), and these maps are distinct from the map for
224 the hallway. Moreover, the fragmentations generated by the online model are consistent
225 with the fragments from the principled baseline method (Fig. 4d compared to Fig. 2e).
226 Because of the stochastic process of map matching and retrieval from memory, new
227 or multiple maps are sometimes formed and retrieved within in the same room (scat-
228 tered gray dots not contained within highlighted gray regions, Fig. 4a-c, bottom). This
229 suggests that there might be more than one map for the same space, even without con-
230 textual changes. This model can be used to generate fragmentations and predicted grid
231 cell tuning curves for arbitrary environmental geometries; we do so for model cells from
232 different grid modules in two environments, Fig. 4e,h (fragmentations of more environ-
233 ments, including a square sprial maze and a simple linear track, shown in SI, Fig. S1a-c).
234 If the angular field is of view ϕ is restricted rather than omnidirectional, the maps also
235 acquire direction tuning, Fig. 4h and Fig. S1c.



236

Figure 4: Online fragmentation results. **A–C Top:** Example trajectory snippets through three different environments (blue line), with current agent position indicated as an open blue circle. Fragmentation events indicated by red dots. The numbers indicate subregions identified in Figure 2E. **A** additionally shows the corresponding predictability signal (blue) and threshold (dashed line). **Bottom:** The same trajectory snippets traversing the internal coding state space. The gray circular areas highlights the most-visited parts of state space for each environment, and the numbers correspond to the mapped area in the environment. Discontinuous jumps in state space, corresponding to transitions between submaps which occur at fragmentation events, are plotted in red. **D:** Heat maps indicating the density of online fragmentation events closely match the offline predictability-based clustering fragmentations from Fig. Figure 2E. The fragmentation decision map can be interpreted as the tuning curve of a “fracture” cell, which in multi-room environments can be interpreted as a “doorway cell” because the fractures happen at doorways. **E:** Firing fields of three simulated grid cells in two distinct environments. C1 and C2 are from a common module; C3 is from a distinct module of larger scale. White lines in bottom left panel show the submap discontinuity between the rooms and hallway. **F:** Evidence for map re-use and fragmentation: *Left:* Spatial cross-correlation of the left and right room representations (by C1 and C3) in the two-room-hallway environment is centered at zero (center of black circle), illustrating that the same map is reused in both rooms across modules. *Right:* Spatial cross-correlation of the right room and hallway representations by C1 (top) and by a control pattern (bottom) that extends to the whole environment (in a continuous way without realignment) C1’s right room tuning curve. **G:** Cross-correlation of comodular cells (C1, C2) in the right room, and in the hallway: the cells have the same relative phase in each map fragment, showing maintained comodular cell-cell relationships within and across all map fragments. **H,I:** Directionally tuned firing fields in the hairpin maze (shown in C) of an idealized grid cell. The difference in firing fields for consecutive arms shows that the arms are mapped to different parts in mapping space depending on the direction they are traversed. The matrices show the correlation coefficients comparing signals of different arms.

237

238 **Coherence of fragmentation across scales and maintenance of cell-cell** 239 **relationships**

240 Two key structural predictions of our model are, first, that the map fragmentations are
241 consistent and coherent across scales (across grid modules), with all cells and modules
242 remapping at the same spatial location in an environment. This is in contrast with
243 eigenvector-based models [20, 21, 34], in which there is no specific or coherent remapping
244 decision that is made across eigenvectors, Fig. S3,S4, Fig. 6.

245 Second, in our model all grid cells within each module maintain fixed cell-cell rela-
246 tionships across map fragments and environments. This too is in direct contrast with
247 eigenvector-based models, Fig. 4g,S5, Fig. 6. Consistent with our model, grid cell data
248 and analyses reveal that the pairwise relationships between co-modular grid cells remain
249 stable across environments [35] and states [36, 37] even when place cells remap and their
250 relationships change. These neural data more generally do not support models in which
251 grid cell responses are derived from place cell responses [34, 38] because they would
252 predict altered cell-cell relationships when place cells remap [36].

253 Efficient planning with fragmentations

254 Next, we quantify the functional utility of map fragmentation in a navigational planning
255 problem. The fragmented maps, which represent a form of state abstraction, decompose
256 the planning problem hierarchically, into a family of smaller and simpler sub-problems.
257 Thus, they are expected to make planning more efficient. We perform computational
258 experiments to illustrate this point, comparing a bi-level navigation algorithm in the
259 fragmented map with a simple baseline.

260 Consider a goal-directed problem in which agents, who have previously mapped the
261 space, are tasked with finding a path to a cued goal location from a start location.
262 For planning, we will assume that the LTM containing stored observation-location as-
263 sociations also includes an explicit submap identification (that is, all observations until
264 a fragmentation event are assigned the same submap ID; at a fragmentation event, if
265 the retrieved map has not yet been assigned a submap ID, a new submap ID is initi-
266 ated and added to the LTM and associated with all subsequent observations until the
267 next fragmentation event, and so on; all the observations between fragmentations are
268 fused using local displacement information to form a submap for the whole fragment)
269 and storing submap transitions. The environments are complex, but *without* repeating
270 submap structure (Fig. 5a-b, d-e), because the fragmented representations generated by
271 our simple agent do not distinguish between difference spaces with the same appearance
272 (no global odometry assumed across submaps).

273 The baseline (global) agent is furnished with a global map, which includes ground-
274 truth position information for all observations (Fig. 5a,d) and uses the Rapidly-exploring
275 Random Tree (RRT) algorithm [39] to find a path through the space (Methods). The
276 agent using a fragmented approach constructs a graph in which the nodes correspond to
277 the submaps, and the edges correspond to observed transitions between submaps during
278 exploration. It performs a depth-first search through the transition tree to find the
279 sequence of submaps that lead to the node containing the target location (determined
280 by querying the LTM with the target inputs). Within each submap, the agent uses the
281 RRT algorithm to plan a path between the locations corresponding to the entry and exit
282 edges. This agent possesses no global positional information.

283 In the environment of Fig. 5a-b, routes are found vastly more rapidly with fragmented
284 maps than without: we see a ~ 5 -fold speedup. The relative advantage of planning with
285 fragmented maps grows superlinearly with the complexity and size of the environment
286 and separation between start and end locations within these spaces, Fig. 5c (right; steps
287 are a proxy for the problem complexity).

288 Next, we simulate agents moving through 3D photorealistic virtual apartments in
289 which observations are rich pixel images with range data, Fig. 5d, g. We apply con-
290 volutional visual recognition networks to the dense inputs to extract sparse landmarks
291 and use these to generate online map segmentations (Methods). As before, the agent
292 performs bi-level planning on the tree of transitions with submaps as nodes and RRT
293 planning within submaps. Here we find a several orders of magnitude speedup in plan-
294 ning with map fragmentation, Fig. 5f.

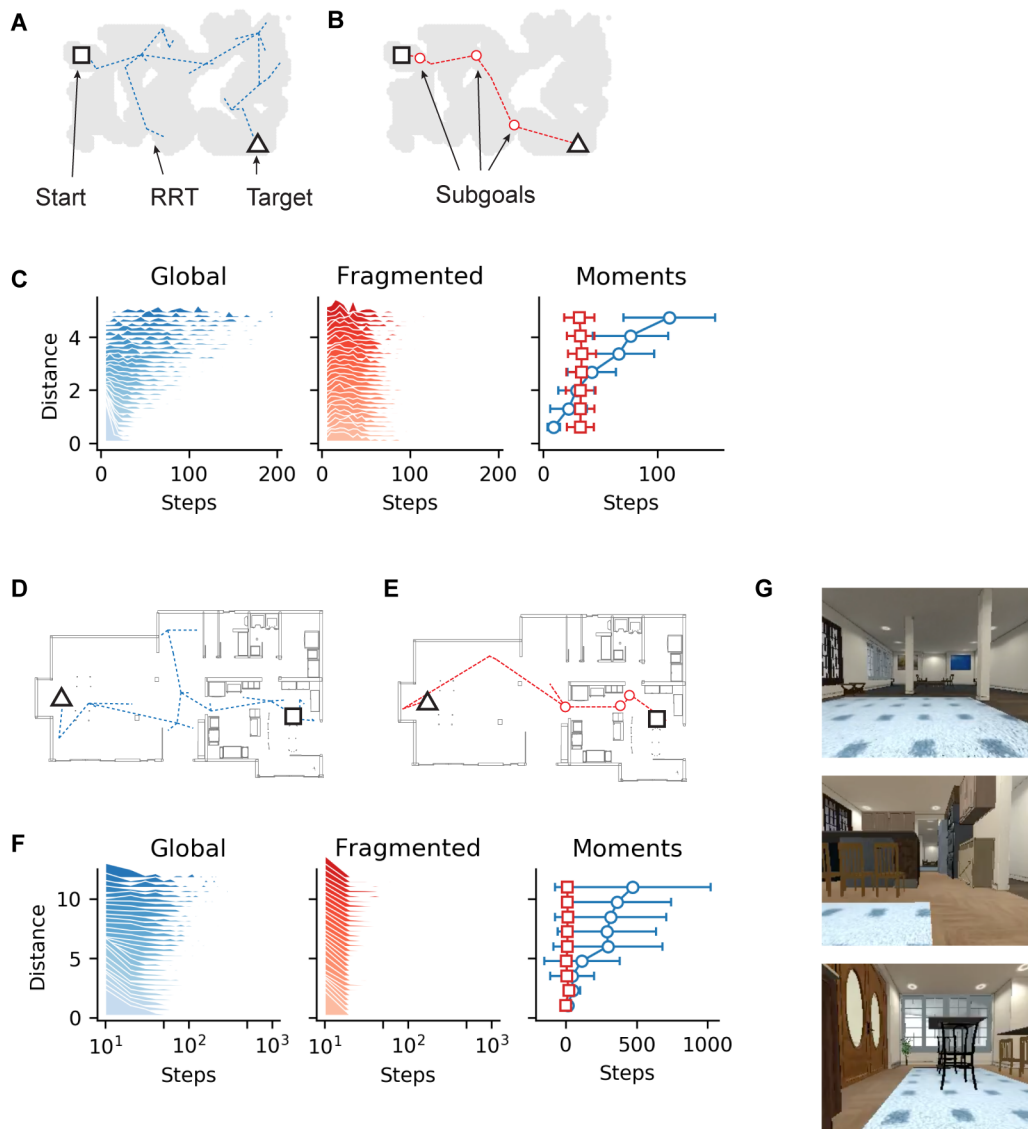


Figure 5: Efficient Hierarchical Planning with Map Fragmentations. **A-C:** Results of the planning algorithm applied to the global map of the environment (A) and to the hierarchical maps from our online fragmentation model (B). In C we plot the distributions of planning steps conditioned on the distance between start and target locations. **D-G:** Similar to A-C but using an alternative fragmentation algorithm based on semantic information extracted from visual inputs as shown in G.

295 Discussion

296 Relationship to existing work

297 Existing models of neural representations in multi-chambered environments fall into
298 three categories, Fig. 6: In the first, fragmentation is driven by path integration errors
299 that cause a large mismatch between estimated position and familiar observations [40];
300 in environments with little ambiguity in the external sensory cues or no path integra-
301 tion errors, there would be no fragmentation. In the second, spatial representations are
302 assumed to be derived directly and entirely from combinations of external cues, thus
303 similar external inputs induce similar representations, but without a notion of map frac-
304 turing or explicit discrete fragmentations [41]. The third category represents positions
305 in an environment as states, and spatial representations as the top eigenvectors of the
306 transition matrix between states (the transition matrix can be defined by how a specific
307 agent or random agent traverses the states) [20, 21]. These models require a global and
308 veridical acquisition of a complete map of the environment and of the transition matrix
309 between all pairs of locations in the environment, before any potential spatial represen-
310 tations can be defined. As in the second category, these also do not provide explicit or
311 discrete fragmentations of the environment; different eigenvectors have different spatial
312 patterns, changing at different spatial frequencies across the space. If two eigenvectors
313 with the same spatial frequency are interpreted as two co-modular grid cells, they do not
314 maintain their cell-cell relationships across the space, in contrast with the known preser-
315 vation of comodular grid cell phase relationships not just within but across environments,
316 time, and behavioral states like waking and sleep [35–37, 42]. By contrast, our model is
317 fully online so that from the very first trajectory in an environment it generates explicit,
318 robust fragmentations of the space at specific discrete locations in each space. It does
319 so by driving a discontinuous and synchronized randomized phase change across all grid
320 modules at the fracture point. These fracture events are determined by a rise in surprisal
321 or prediction error. This induces fractures across regions whose geometries are quite dis-
322 tinct, e.g. a doorway, a u-turn in the hairpin maze, or a narrowed hall-like passage in
323 the organically shaped environment (cf. Fig. 4). The fragmentations are predicted to
324 occur even in the absence of positional ambiguity from path integration error, preserve
325 co-modular phase relationships across all map fragments, and require a much smaller
326 time and memory demand than transition matrix models. Finally, the model involves
327 only simple, biologically plausible computational elements, with grid cells and BVCs,
328 a short-term memory, and a long-term memory, to explain a number of experimental
329 results.

330 Our work, initially motivated by the empirical observations of fragmented maps in
331 neuroscience, is closely related to work on segmented maps in the field of simultaneous
332 localization and mapping (SLAM) in robotics [19, 43–45]. The main difference is that
333 predictions in our model are based on a temporally limited window into the past, pro-
334 vided through the STM, whereas in [19] *all* observations are accumulated into a map
335 that the prediction is based on. Further, our predictions are based on idiothetically-
336 centered local views of the environment (BVC) – which are not assembled into a global

337 allocentric map – and use an adapted moving average as a STM. For (re-)localization
338 we use local views stored in a spatially indexed LTM.

339 As we have shown, spatial abstraction and spatial hierarchy in the form of map frag-
340 ments can be of high utility in efficient search for solving goal-directed problems. State
341 abstractions and hierarchical representations are broadly recognized to be important for
342 more efficient reinforcement learning as well, and implemented in different forms includ-
343 ing the classic options framework and more recent attempts [46, 47]. A key challenge for
344 such approaches is to find rules that generate appropriate state abstractions, especially
345 those capable of doing so in an online or streaming way. Our work is a contribution in
346 this direction; related work includes the generation of temporal abstractions based on
347 novelty rather than surprisal [48].

348 Our use of a surprisal signal is closely related to curiosity-based algorithms for rein-
349 forcement learning [49]. These algorithms use prediction error as an internal reward, to
350 drive agents to explore unknown parts of the space. By contrast, we use prediction error
351 as a way to generate state abstractions.

352 **Model extensions: a broader set of metrics for fragmentation**

353 The general principle of online state abstraction through online map fragmentation can
354 use metrics in addition to surprisal for triggering a fragmentation event. Consider the
355 case of two hallways with similar ideothetically-centered views, e.g. hallways 2 and 3 in
356 Fig. 4c, that differ only in the permitted turn direction at the end. A natural extension of
357 the model would be to incorporate a cell population encoding navigational affordances, to
358 fragment and select maps based not only sensory surprisal but also on the set of actions
359 that can be or are commonly taken. Other extensions include using the physical distance
360 between states [20, 21], the passage of time [50–52] with a dynamic (temporally decaying)
361 threshold for fragmentation that makes fragmentation more likely as time elapses (also
362 see [19]), the appearance unique or novel visual features including landmarks [48, 53–55],
363 and sufficient mismatch in the estimates of state made from different cues or sensory
364 modalities [40, 56], in addition to the metric of perceptual predictability that we have
365 used here and that the hippocampus has been shown to be sensitive to [57, 58]. The
366 present model, which provides an online method for generating meaningful abstractions,
367 may be applied with arbitrary combinations of these metrics to generate fragmentations
368 influenced by multiple factors.

369 **Merging of maps**

370 In case of prolonged experience in the two compartment environment, map fragmenta-
371 tions tend to merge into a single, continuous representation that covers both compart-
372 ments [14]. In our model some map fragments can, because of the stochastic nature
373 of the fragmentation process, occasionally extend beyond an expected fragmentation
374 boundary (see Fig. S1d). These events occur sparsely and are unlikely to be the source
375 of the merging of maps observed in [14]. We expect the merging of maps to result from
376 an improvement of the prediction signal with more experience, which can be modeled

377 by allowing the prediction system to use not just recent observations from short term
378 memory, but also past observations from long term memory. Exploring the dynamics of
379 this process is an interesting potential extension of the present work.

380 **Role of map fragmentation for general cognitive representation**

381 Our model of online fragmentation of a continuous stream of experience enables the
382 representation of a very general class of maps – including in spatial and non-spatial
383 cognitive domains – in a way that exceeds the capabilities of a “pure” grid code. Grid
384 cells generate Euclidean representations of Euclidean spaces [11]. Fragmented maps can
385 each be viewed as separate local Euclidean “charts”, mapped out by a multi-modular
386 grid code, that are then associated to each other through transitions learned in the hip-
387 pocampus according to the global layout of the charts. In other words, the combination
388 of fragmented maps and the transitions between them can be viewed as a topological
389 atlas [59] or topometric map [60], that can represent highly non-Euclidean structures
390 while also permitting locally metric computations.

391 Thus, from a general perspective, map fragmentation and remapping (reanchoring)
392 on cognitive representations can be viewed as facilitating the step from representing
393 flat Euclidean space to representing richer manifolds. In combination with grid cells’
394 ability to represent high-dimensional variables [11], such a coding scheme becomes highly
395 expressive.

396 In contrast to the approach taken in [12, 61] there is no need to generate entirely new
397 neural codes and representations to fit the local statistics of ea explored space. Instead,
398 we propose that the neural codes seen within submaps retain their native structure across
399 spaces, in the form of a pre-formed and stable recurrent scaffold for memory through
400 grid cells. Even though grid cell representations in each module are 2-dimensional,
401 theoretically the set of modules an represent even high-dimensional continuous spaces
402 [11], while potential non-Euclidean aspects of cognitive varaibles can be captured by
403 the between-submap transitions. This structuring of memory into continuous parts
404 with preexisting scaffolds [62–66] together with occasional transitions between these
405 continuous chunks simultaneously provides rapid learning and flexibility.

406 **Episodic memory**

407 Episodic memory, one example of a general cognitive representation, deserves special dis-
408 cussion because of the privileged role of the hippocampal system in its creation, storage,
409 and use [67, 68]. Like spatial map fragmentations, episodic memory involves fracturing
410 the continuous stream of temporal experience into chunks that involve similar percep-
411 tual, temporal, and contextual elements [3–5, 69]. Thus, our proposal for surprisal- or
412 prediction-error based spatial segmentation can, with minimal modifications, be applied
413 to study memory chunking. Interestingly, the memory for non-spatial items has also been
414 shown to segment based on changes in spatial context, specifically by passage through
415 doorways [70], as would be predicted by the present model.

416 The utility of applying our model first in the spatial domain is that it yielded concrete

417 predictions that we found to be quantifiably consistent with observed neural representa-
418 tions and map fragmentations. Applying it next across cognitive domains will contribute
419 to a unified computational model for how the hippocampal formation generates struc-
420 tured memories of spatial and non-spatial cognitive experience [12, 18, 61, 68, 69, 71,
421 72], and how these fragmented representations could permit more efficient and flexible
422 use of memory for cognitive problem solving.

423 **Experimental Predictions**

424 The decision to form a new map fragment in our model depends only on recent observa-
425 tions that are filtered through a STM, without requiring global information about the
426 environment. Thus, map fragmentations are predicted to occur in real time and on the
427 very first pass through relevant regions of new environments, consistent with experi-
428 mental results in the spatial and non-spatial domains [3–5, 73]. Further, in our model,
429 all grid cells and grid modules undergo map fragmentation simultaneously, at the same
430 time and location along a given trajectory, unlike in other models (Fig. S3,S4) [20, 21].

431 Fragmentations tend to occur at spatial bottlenecks that limit the prediction horizon,
432 which correspond to “doorways” in the environment. The current evidence for cells
433 firing at doorways is mixed [74, 75]. However, the necessity for a neural correlate that
434 communicates the fragmentation decision and facilitates across-module grid realignment
435 under a fragmentation event predicts the existence of “fracture cells” whose tuning curves
436 would resemble the heatmaps of Fig. 4d, which in these environments are consistent with
437 an interpretation as “doorway cells”. Note that regions at which a fracture cell would
438 be active can correspond to locations with quite dissimilar local geometries, as seen
439 in the fracture locations across three distinct contexts in Fig. 4d; thus, fracture cell
440 tuning curves are not merely an instance of place field repetition caused by similar local
441 geometries [41].

442 A common theme in MEC seems to be that cells with spatially structured tuning
443 coexist with vector versions of themselves: i.e., cells that have similar tuning curves
444 but are offset by a fixed vector (e.g. BVCs [26, 27] and landmark or object vector cells
445 [76, 77]). In this light we might also expect “fragmentation vector cells” or “doorway
446 vector cells” that fire if the rodent is at a fixed angle and distance from a fragmentation
447 location. These cells, which could be interpreted as encoding future action affordances
448 or future map transitions, would facilitate planning.

449 Next, the model predicts that the stochastic process of generating map fragmentations
450 can result in more than one map for the same region even when there is not an explicit
451 manipulation of context or task. There are at least two implications of this result. First,
452 it suggests that variations in the firing of grid and place cells on different visits to a
453 location might be due not only to variable paths taken within a single map [78] but to
454 the retrieval of entirely different maps. Second, these multiple, stochastically generated
455 maps might subsequently be easy to harness for contextual differentiation, for instance
456 like “splitter” cells [61, 79–81].

457 Finally, the large efficiencies in planning and goal-directed navigation afforded by the
458 use of fragmented maps suggest that neural planning should exhibit hallmarks of the

459 fragmentation process: If theta phase precession or waking neural replay events [82–88]
460 correspond to planning [89–91], we should expect them to exhibit punctate trajecto-
461 ries with hierarchical dynamics between versus within fragments in multicompartment
462 environments.

463 Methods

464 Data and code availability

465 The source code will be made available on request and posted online upon publication.

466 Offline fragmentations from predictability and surprise

467 We approximate the probabilistic observation model $P(z' | x', x, z)$ by

$$P(z' | x', x, z) = \int P(z' | x, m) P(m | x, z) dm \approx P(z' | x', m_{x,z}^*).$$

468 Here $m_{x,z}^*$ is the maximum a posteriori estimation of an occupancy map given by an
469 inverse sensor model as described in [29], and $P(z' | x, m)$ is the respective range sensor
470 model. More precisely: Given a deterministic range sensor that takes measurements
471 along a fixed number ($n = 1000, 1500$) of simulated beams, whose angles are chosen at
472 equally spaced angles from the interval $[-\pi, \pi]$, we take three depth measurements $z, z',$
473 and z'' . The first two are taken in the actual environment at their respective poses x
474 and x' , whereas the third is taken on a map $m_{x,z}^*$ built from the initial measurement z
475 made at x . The observation model $P(z' | x, m)$ is then defined as a multivariate diagonal
476 Gaussian with constant diagonal entries $\sigma = 1.0$ and mean z'' , Fig. 2a,b.

477 The function underlying the distance matrix used for the Isomap embedding (cf.
478 Fig. 2d) is given by the *mutual surprise* $s(x, x')$ between two poses x, x' which we define
479 as

$$s(x, x') := -\frac{1}{2} \left(\log P(z | x, x', z') + \log P(z' | x', x, z) \right).$$

480 We refer to the negative mutual surprise as *mutual predictability*. With this in hand
481 we define the *average surprise* $s(x) = s(x; r, \varepsilon)$ of a pose by averaging over the mutual
482 surprise about all poses at a fixed distance. To be more precise we define

$$s(x) := \frac{1}{|\Delta(x)|} \sum_{\Delta(x)} s(x, x'),$$

483 where $\Delta_x = \Delta_x(r, \varepsilon)$ is the set of all poses whose distance to x lies in the range $[r - \varepsilon, r + \varepsilon]$,
484 for some previously fixed $r, \varepsilon > 0$; in our experiments we use $r \approx 0.4$ and $\varepsilon \approx 0.05$
485 depending of the minimal distances between poses. We sometimes refer to the negative
486 average mutual surprise as *contiguity*. Informally, a high contiguity implies fewer surprises
487 in direct proximity of the current pose and thus a low urge to remap.

488 To extract map fragmentations we uniformly sample poses from the environment and
489 compute their average surprise, Fig. 2e. We then consider only those poses whose

490 surprise lies below a previously fixed threshold (chosen accordingly for each environment).
 491 To make an informed choice about the threshold we compute a discrete contour tree
 492 [24] of the poses with respect to the average surprise visualizing the evolution of the
 493 connectivity with respect to increasing thresholds, Fig. 2f. The connected components
 494 of the subthreshold region yields a fragmentation into sub-maps, one for each connected
 495 region, and a suprathreshold transition region. We consider two poses to be connected
 496 if their Euclidean distance is below another previously fixed threshold that depends on
 497 the coverage of the environment by all the pose samples.

	Fragmentation w/o Sensor Ambiguity	Fragmentation on 1 st Visit	Memory Demand	Coherent Fragm.	Cell-Cell corr. preserved
Spatial codes from BVC	No	YES	n	YES	YES
Laplacian & SR	YES	No	n²	No	No
Our model	YES	YES	n	YES	YES

Figure 6: Comparison to other models. Our model improves on the potential shortcomings of other mapping approaches. Examples for model based on spatial codes derived from BVCs are [40, 41], and for models based on SR or graph Laplacian are [20, 21].

498 Online fragmentations from predictability

499 Observations and internal mapping locations

500 As before, our observation model is given by a range sensor that takes measurements
 501 along a fixed number of simulated beams. The beams' angles are chosen at equally
 502 spaced angles from the interval $[\theta_t - \phi/2, \theta_t + \phi/2]$. Here θ_t denotes the head direction at
 503 time t and $\phi = 360^\circ, 270^\circ$ defines the field of view of the agent; cf. Fig. 3a. We convert
 504 these range measurements into the activity z_t of a simulated population of boundary
 505 vector cells by a binning process; cf. Fig. 3a,c. In our model we assume there is a $n \times n$
 506 array of BVCs covering an area of $w \times w$, with $n = 91, 111$ and $w \approx 4\text{m}$.

507 We assume that internally locations are represented by a population of idealized grid
 508 cells of multiple scales. For ease of computation, we interpret this multi-module grid code
 509 as a high capacity code for an unfolded 2-dimensional space [11]; cf. Fig. 4a-c (bottom).
 510 The Poisson rate maps f_c for an idealized grid cell c are then generated from superposing
 511 three cosinusoidal waves, each offset by an angle of 60° , over the unfolded 2-dimensional
 512 grid space, i.e.

$$f_c(x) := \frac{4\pi}{\sqrt{3}\lambda_c} \sum_{k=0}^2 \left[1 + \cos(\langle R_c(x - x_c), e^{-ik\frac{\pi}{3}} \rangle) \right].$$

513 Here λ_c and x_c encode the lattice scale and its offset, and R_c is a rotation matrix defining
 514 the orientation of the lattice.

515 **Short term memory:**

516 The short term memory (STM) is defined as an adapted exponential moving average of
 517 BVC activity:

$$m_t := \alpha \cdot \frac{\hat{z}_t}{\|\hat{z}_t\|} + (1 - \alpha) \cdot \frac{z_t}{\|z_t\|},$$

518 where the prediction

$$\hat{z}_t := \text{shift}(m_{t-1}, -\lambda v_{t-1})$$

519 is a shifted version of the 2d-array m_{t-1} with respect to the scaled velocity of the agent.
 520 We found that a smoothing parameter $\alpha \approx 0.9$ works well. The scaling parameter $\lambda = \frac{n}{w}$
 521 maps from the environment into pixel space. The shift of the BVC array results in a
 522 diffused version of the array caused by shifts with non-integer values. The extent of
 523 diffusion depends on the resolution (or number) of the BVCs.

524 **Prediction model and fragmentation events**

525 The prediction model is a normalized dot product of the current BVC observation z_t
 526 with the prediction \hat{z}_t computed from the STM as described above:

$$\mathbb{P}(z_t | m_{t-1}, v_{t-1}) \propto \frac{\text{vec}(z_t)}{\|\text{vec}(z_t)\|} \cdot \frac{\text{vec}(\hat{z}_t)}{\|\text{vec}(\hat{z}_t)\|}^\top$$

527 where $\text{vec}(z)$ is the unfolded version of a 2d-array z ; cf. Fig. 3b-d. A fragmentation event
 528 is triggered after the prediction signal $\mathbb{P}(z_t | m_{t-1})$ recovers from falling below a fixed
 529 threshold θ ($\approx 0.9, 0.925$) and rises above again; cf. Fig. 3b. The normalization and the
 530 fact that both z_t and \hat{z}_t are non-negative ensures that the prediction score lies within
 531 the intervall $[0, 1]$.

532 **Long term memory and relocalization**

533 The LTM is implemented as a matrix $M \in \mathbb{R}^{n \times S}$ whose s 'th column is given by the
 534 concatenation of the internal position estimate x_{t_s} , its predecessor x_{t_s-1} and the state
 535 m_{t_s} of the STM at the time t_s the entry was written to memory, i.e. we have (cf. Fig. 3e)

$$M_{*,s} := (\text{vec}(x_{t_s}) \text{vec}(x_{t_s-1}) \text{vec}(m_{t_s}))^\top.$$

536 We fill the memory as follows: At each time step t we choose a slot (column) s_t in the
 537 memory and replace the corresponding entry with the new one. Until we reach capacity,
 538 that is as long as $t \leq S$, we set $s_t = t$, after that the slots s_t are chosen uniformly at
 539 random – similar to the associative memory in [92]. Thus, the LTM consists of two
 540 associative memories: one storing associations between locations and observations, and
 541 the other storing state transitions. Alternatively, one could store associations with the

542 actual observations z_{t_s} and not the filtered observations from the STM m_{t_s} , but we found
 543 that the associations with the STM work better and result in more stable fragmentations.
 544 The same is true when we restrict the capacity of the memory; cf. Fig. S6. Note that the
 545 LTM also maintains a temporal memory storing transitions (x_{t_s-1}, x_{t_s}) for each entry in
 546 the memory. We use a memory size S between 2000 and 6000.

547 To determine the new location during a fragmentation event we query the LTM and
 548 compute two distinct weight vectors w_1 and w_2 . The first encodes how well a given
 549 observation z fits any of its entries and is given by

$$w_1(s, z; M) = \theta_M(\text{vec}(m_{t_s}) \cdot \frac{\text{vec}(z)}{\|\text{vec}(z)\|}^\top).$$

550 With slight abuse of notation we denote by θ_M the function that sets all values below
 551 a certain threshold θ_M to $-\infty$. For ease of notation we set $e^{-\infty} := 0$ – this becomes
 552 relevant in the probability computation below. We usually set this threshold to be equal
 553 to the fragmentation threshold $\theta \approx 0.93$. In order to allow for more flexibility during
 554 the above lookup we query the LTM not only with the actual observation z , but also
 555 with observations shifted by small pixel offsets δ , i.e. with $z_\delta = \text{shift}(z, \delta)$ instead of
 556 just z , where $\delta \in \mathbb{Z}^2$ is chosen from a small region Δ around the origin. If a shifted
 557 observation fits a particular entry in the memory better, we replace the corresponding
 558 entry in the computed weight vector w_1 . Then, if one of these adjusted entries, s say, is
 559 chosen during a remapping event we do not remap exactly to the associated position x_{t_s}
 560 but adjust it proportional to the respective offset δ and remap to $x_{t_s} + \frac{1}{\lambda}\delta$ (recall that
 561 λ translates from environment to pixel coordinates).

562 The second vector serves as a bias towards map transitions that have already been
 563 traversed and is given by

$$w_2(s, x; M) = \exp\left(-\frac{\|x - x_{t_s-1}\|^2}{0.25}\right).$$

564 Note that we use the Euclidean norm between two 2d vectors out of computational con-
 565 venience, but we could have used the dot product of their corresponding multi modular
 566 grid codes as well. Finally, when a fragmentation event is triggered we sample a new
 567 location from

$$P(x | z; M) \propto e^{\tau \cdot w_0} \cdot P_0(x) + \sum_s e^{\tau \cdot (w_1(s, z) + w_2(s, x))} \cdot \delta(x_{t_s}),$$

568 where $P_0(x)$ is a distribution over the space of possible locations, $w_0 = 1$ the concentra-
 569 tion parameter, and $\tau = 1, 10, 20$ is the inverse temperature of the model; cf. Fig. 3g.

570 Trajectories

571 The trajectories are generated by choosing waypoints in the environment uniformly at
 572 random and navigating toward the next waypoint along a perturbed shortest path at a
 573 mean speed of 20 cm/sec. Time is discretized into steps of size $\Delta t = 0.1$ sec.

574 Hierarchical Planning

575 We apply Rapidly-exploring Random Trees (RRT) [39] to find a path between randomly
576 chosen pairs of start and target positions, Fig. 5a. Next, we run our online segmentation
577 algorithm to get an environment-fragmentation into submaps and form a topological
578 graph whose vertices and edges correspond to submaps and transitions respectively.
579 For each map-fragment we superpose all its associated memories (STM-filtered BVC
580 activity) and threshold this newly formed representation to form an occupancy grid
581 map (in the sense of [29]) which we can apply the path planning algorithm to. We
582 exploit the hierarchical structure by first finding a path of transitions in the topological
583 graph, using a breadth-first search, and reduce the overall planning task into a family
584 of sub-problems as follows: Each transition into- and out of a node defines a pair of
585 local entry and exit positions on the submap associated with the traversed node defining
586 a smaller planning problem that can be solved more effectively, Fig. 5b. In Fig. 5c we
587 plot the distances between start and goal locations against the number of planning steps
588 needed.

589 The algorithm underlying the results in Fig. 2d–g is given as follows. Because the
590 3D environments involve dense observations of pixel-rich data, we add image processing
591 and observation sparsification steps in the form of landmark identification. The agent
592 receives RGB-D images as input, removes the floor plane, and segments the resulting
593 point cloud. It retains as landmarks the large segments that are not vertical walls, which
594 are generally large furniture items that are both relatively static and easy to recognize
595 robustly from new viewpoints. As it moves through the environment, fragments are
596 defined as follows: Starting at the initial location, the current fragment is defined a set of
597 two visible landmarks, and the region of space from which both those landmarks remain
598 in view constitutes the set of spatial locations assigned to that fragment. Whenever
599 the agent moves into a part of the space where one or both of those landmarks are not
600 visible, and if the current location does not correspond to any existing fragment, it starts
601 a new fragment. Each fragment is connected topologically to the fragment it entered
602 from.

603 Arm-arm correlation

604 The correlation matrices in Fig. 4i are computed as follows. For each arm in Fig. 4h
605 we produce a 1-dimensional signal by averaging over the x-axis of the respective tuning
606 curves in each arm. Each entry c_{ij} in the matrix is then given by the Pearson correlation
607 coefficient of the 1-dimensional signals in arm i and j .

608 References

- 609 1. Julian, J. B., Keinath, A. T., Marchette, S. A. & Epstein, R. A. The Neurocognitive
610 Basis of Spatial Reorientation. *Curr Biol* **28**, R1059–R1073 (Sept. 2018).

- 611 2. Levy, R., Reali, F. & Griffiths, T. L. *Modeling the Effects of Memory on Human*
612 *Online Sentence Processing with Particle Filters in Proceedings of the 21st Interna-*
613 *tional Conference on Neural Information Processing Systems* (Curran Associates
614 Inc., Vancouver, British Columbia, Canada, 2008), 937–944.
- 615 3. Swallow, K. M., Zacks, J. M. & Abrams, R. A. Event boundaries in perception affect
616 memory encoding and updating. *J Exp Psychol Gen* **138**, 236–57 (May 2009).
- 617 4. Ezzyat, Y. & Davachi, L. What constitutes an episode in episodic memory? *Psychol*
618 *Sci* **22**, 243–52 (Feb. 2011).
- 619 5. Baldassano, C. *et al.* Discovering Event Structure in Continuous Narrative Percep-
620 tion and Memory. *Neuron* **95**, 709–721.e5 (Aug. 2017).
- 621 6. Hafting, T., Fyhn, M., Molden, S., Moser, M.-B. & Moser, E. Microstructure of a
622 spatial map in the entorhinal cortex. eng. *Nature* **436**, 801–806 (2005).
- 623 7. Whishaw, I. Q., Hines, D. J. & Wallace, D. G. Dead reckoning (path integration)
624 requires the hippocampal formation: evidence from spontaneous exploration and
625 spatial learning tasks in light (allothetic) and dark (idiothetic) tests. eng. *Behav*
626 *Brain Res* **127**, 49–69 (2001).
- 627 8. Blum, K. I. & Abbott, L. F. A model of spatial map formation in the hippocampus
628 of the rat. eng. *Neural Comput* **8**, 85–93 (1996).
- 629 9. Burak, Y. & Fiete, I. R. Accurate path integration in continuous attractor network
630 models of grid cells. *PLoS Comput Biol* **5**, e1000291 (Feb. 2009).
- 631 10. Banino, A. *et al.* Vector-based navigation using grid-like representations in artificial
632 agents. *Nature* **557**, 429–433 (May 2018).
- 633 11. Klukas, M., Lewis, M. & Fiete, I. Efficient and flexible representation of higher-
634 dimensional cognitive variables with grid cells. *PLoS Comput Biol* **16**, e1007796
635 (Apr. 2020).
- 636 12. Whittington, J. C. R. *et al.* The Tolman-Eichenbaum Machine: Unifying Space
637 and Relational Memory through Generalization in the Hippocampal Formation.
638 *Cell* **183**, 1249–1263.e23 (Nov. 2020).
- 639 13. Derdikman, D. *et al.* Fragmentation of grid cell maps in a multicompartment en-
640 vironment. *Nat Neurosci* **12**, 1325–1332 (Oct. 2009).
- 641 14. Carpenter, F., Manson, D., Jeffery, K., Burgess, N. & Barry, C. Grid cells form
642 a global representation of connected environments. *Curr Biol* **25**, 1176–82 (May
643 2015).
- 644 15. Colgin, L. L., Moser, E. I. & Moser, M.-B. Understanding memory through hip-
645 pocampal remapping. *Trends Neurosci* **31**, 469–77 (Sept. 2008).
- 646 16. Fyhn, M., Hafting, T., Treves, A., Moser, M.-B. & Moser, E. I. Hippocampal remap-
647 ping and grid realignment in entorhinal cortex. eng. *Nature* **446**, 190–194 (2007).
- 648 17. Colgin, L. L. *et al.* Attractor-map versus autoassociation based attractor dynamics
649 in the hippocampal network. *J Neurophysiol* **104**, 35–50 (July 2010).

- 650 18. Sanders, H., Wilson, M. A. & Gershman, S. J. Hippocampal remapping as hidden
651 state inference. *Elife* **9** (June 2020).
- 652 19. Fairfield, N., Wettergreen, D. & Kantor, G. Segmented SLAM in three-dimensional
653 environments. *Journal of Field Robotics* **27**, 85–103 (2010).
- 654 20. Machado, M. C., Bellemare, M. G. & Bowling, M. H. A Laplacian Framework for
655 Option Discovery in Reinforcement Learning. *CoRR* **abs/1703.00956** (2017).
- 656 21. Stachenfeld, K. L., Botvinick, M. M. & Gershman, S. J. The hippocampus as a
657 predictive map. *Nat Neurosci* **20**, 1643–1653 (Nov. 2017).
- 658 22. Tenenbaum, J. B., Silva, V. d. & Langford, J. C. A Global Geometric Framework
659 for Nonlinear Dimensionality Reduction. *Science* **290**, 2319–2323 (2000).
- 660 23. Ester, M., Kriegel, H.-P., Sander, J. & Xu, X. *A Density-Based Algorithm for*
661 *Discovering Clusters in Large Spatial Databases with Noise* in *Proceedings of the*
662 *Second International Conference on Knowledge Discovery and Data Mining* (AAAI
663 Press, Portland, Oregon, 1996), 226–231.
- 664 24. Edelsbrunner, H. & Harer, J. *Computational Topology - an Introduction*. I–XII,
665 1–241 (American Mathematical Society, 2010).
- 666 25. Zacks, J. M. *et al.* Human brain activity time-locked to perceptual event boundaries.
667 *Nat Neurosci* **4**, 651–5 (June 2001).
- 668 26. Barry, C. *et al.* The boundary vector cell model of place cell firing and spatial
669 memory. *eng. Rev Neurosci* **17**, 71–97 (2006).
- 670 27. Lever, C., Burton, S., Jeewajee, A., O’Keefe, J. & Burgess, N. Boundary vector
671 cells in the subiculum of the hippocampal formation. *eng. J Neurosci* **29**, 9771–
672 9777 (2009).
- 673 28. Julian, J. B., Ryan, J., Hamilton, R. H. & Epstein, R. A. The Occipital Place Area
674 Is Causally Involved in Representing Environmental Boundaries during Navigation.
675 *Curr Biol* **26**, 1104–9 (Apr. 2016).
- 676 29. Thrun, S., Burgard, W. & Fox, D. *Probabilistic Robotics (Intelligent Robotics and*
677 *Autonomous Agents)* (The MIT Press, 2005).
- 678 30. Aldous, D. J. *Exchangeability and related topics* in *École d’Été de Probabilités de*
679 *Saint-Flour XIII — 1983* (ed Hennequin, P. L.) (Springer Berlin Heidelberg, Berlin,
680 Heidelberg, 1985), 1–198.
- 681 31. Schaeffer, R., Bordelon, B., Khona, M., Pan, W. & Fiete, I. Efficient online inference
682 for nonparametric mixture models. *Proceedings of Machine Learning Research* (**to**
683 **appear**) (2021).
- 684 32. Blei, D. M. & Frazier, P. I. Distance Dependent Chinese Restaurant Processes.
685 *Journal of Machine Learning Research* **12**, 2461–2488 (2011).
- 686 33. Gershman, S. J., Frazier, P. I. & Blei, D. M. Distance Dependent Infinite Latent
687 Feature Models. *IEEE Trans Pattern Anal Mach Intell* **37**, 334–45 (Feb. 2015).

- 688 34. Dordek, Y., Soudry, D., Meir, R. & Derdikman, D. Extracting grid cell character-
689 istics from place cell inputs using non-negative principal component analysis. *Elife*
690 **5**, e10094 (Mar. 2016).
- 691 35. Yoon, K., Buice, M., Barry C. and Hayman, R., Burgess, N. & Fiete, I. Specific evi-
692 dence of low-dimensional continuous attractor dynamics in grid cells. *Nat Neurosci*
693 **16**, 1077–84 (Aug. 2013).
- 694 36. Trettel, S., Trimper, J., Hwaun, E., Fiete, I. & Colgin, L. Grid cell co-activity
695 patterns during sleep reflect spatial overlap of grid fields during active behaviors.
696 *Nat Neurosci* **22**, 609–617 (Apr. 2019).
- 697 37. Gardner, R. J., Lu, L., Wernle, T., Moser, M.-B. & Moser, E. I. Correlation struc-
698 ture of grid cells is preserved during sleep. *Nat Neurosci* **22**, 598–608 (Apr. 2019).
- 699 38. Kropff, E. & Treves, A. The emergence of grid cells: intelligent design or just
700 adaptation? *Hippocampus* **18** (2008).
- 701 39. LaValle, S. Rapidly-exploring random trees : a new tool for path planning. *The*
702 *annual research report* (1998).
- 703 40. Cheung, A. Probabilistic Learning by Rodent Grid Cells. *PLoS Comput Biol* **12**
704 (2016).
- 705 41. Grieves, R., Duvelle, E. & Dudchenko, P. A boundary vector cell model of place
706 field repetition. *Spatial Cognition Computation* **18**, 1–40 (Mar. 2018).
- 707 42. Gardner, R. J. *et al.* Toroidal topology of population activity in grid cells (Feb.
708 2021).
- 709 43. Kuipers, B. The spatial semantic hierarchy. *Artificial intelligence* **119**, 191–233
710 (2000).
- 711 44. Bosse, M. *et al.* An atlas framework for scalable mapping in 2003 *IEEE Interna-*
712 *tional Conference on Robotics and Automation (Cat. No. 03CH37422)* **2** (2003),
713 1899–1906.
- 714 45. Kuipers, B., Modayil, J., Beeson, P., MacMahon, M. & Savelli, F. *Local metrical*
715 *and global topological maps in the hybrid spatial semantic hierarchy* in *IEEE In-*
716 *ternational Conference on Robotics and Automation, 2004. Proceedings. ICRA'04.*
717 *2004* **5** (2004), 4845–4851.
- 718 46. Sutton, R. S., Precup, D. & Singh, S. Between MDPs and semi-MDPs: A framework
719 for temporal abstraction in reinforcement learning. *Artificial Intelligence* **112**, 181–
720 211 (1999).
- 721 47. Bacon, P.-L., Harb, J. & Precup, D. *The Option-Critic Architecture* in *Proceedings*
722 *of the Thirty-First AAAI Conference on Artificial Intelligence* (AAAI Press, San
723 Francisco, California, USA, 2017), 1726–1734.
- 724 48. Şimşek, Ö. & Barto, A. G. *Using relative novelty to identify useful temporal abstrac-*
725 *tions in reinforcement learning* in *Twenty-first international conference on Machine*
726 *learning - ICML '04* (ACM Press, 2004).

- 727 49. Pathak, D., Agrawal, P., Efros, A. A. & Darrell, T. *Curiosity-Driven Exploration*
728 *by Self-Supervised Prediction in Proceedings of the IEEE Conference on Computer*
729 *Vision and Pattern Recognition (CVPR) Workshops* (July 2017).
- 730 50. Sahay, A., Wilson, D. A. & Hen, R. Pattern separation: a common function for new
731 neurons in hippocampus and olfactory bulb. *Neuron* **70**, 582–8 (May 2011).
- 732 51. Denny, C. A. *et al.* Hippocampal memory traces are differentially modulated by
733 experience, time, and adult neurogenesis. *Neuron* **83**, 189–201 (July 2014).
- 734 52. Ziv, Y. *et al.* Long-term dynamics of CA1 hippocampal place codes. *Nat Neurosci*
735 **16**, 264–6 (Mar. 2013).
- 736 53. Knight, R. Contribution of human hippocampal region to novelty detection. *Nature*
737 **383**, 256–9 (Sept. 1996).
- 738 54. Antunes, M. & Biala, G. The novel object recognition memory: neurobiology, test
739 procedure, and its modifications. *Cogn Process* **13**, 93–110 (May 2012).
- 740 55. Du, Y., Fan, X., Lozano-Perez, T. & Kaelbling, L. Large Scale Robotic Navigation
741 with Spatial Landmarks. *In Preperation* (2021).
- 742 56. Lee, I., Yoganarasimha, D., Rao, G. & Knierim, J. J. Comparison of population
743 coherence of place cells in hippocampal subfields CA1 and CA3. *Nature* **430**, 456–
744 459 (2004).
- 745 57. Kumaran, D. & Maguire, E. A. An unexpected sequence of events: mismatch de-
746 tection in the human hippocampus. *PLoS Biol* **4**, e424 (Nov. 2006).
- 747 58. Lee, I., Hunsaker, M. R. & Kesner, R. P. The role of hippocampal subregions in
748 detecting spatial novelty. *Behav Neurosci* **119**, 145–53 (Feb. 2005).
- 749 59. Lee, J. M. *Introduction to Smooth Manifolds* (Springer New York, 2012).
- 750 60. Badino, H., Huber, D. & Kanade, T. *Visual topometric localization in 2011 IEEE*
751 *Intelligent Vehicles Symposium (IV)* (2011), 794–799.
- 752 61. George, D. *et al.* Clone-structured graph representations enable flexible learning
753 and vicarious evaluation of cognitive maps. *Nat Commun* **12**, 2392 (Apr. 2021).
- 754 62. Farooq, U. & Dragoi, G. Emergence of preconfigured and plastic time-compressed
755 sequences in early postnatal development. *Science* **363**, 168–173 (Jan. 2019).
- 756 63. Dragoi, G. & Tonegawa, S. Preplay of future place cell sequences by hippocampal
757 cellular assemblies. *Nature* **469**, 397–401 (Jan. 2011).
- 758 64. Dragoi, G. & Tonegawa, S. Selection of preconfigured cell assemblies for repre-
759 sentation of novel spatial experiences. *Philos Trans R Soc Lond B Biol Sci* **369**,
760 20120522 (Feb. 2014).
- 761 65. Yim, M. Y., Sadun, L. A., Fiete, I. R. & Taillefumier, T. Place-cell capacity and
762 volatility with grid-like inputs. *Elife* **10** (May 2021).
- 763 66. McKenzie, S. *et al.* Preexisting hippocampal network dynamics constrain optoge-
764 netically induced place fields. *Neuron* **109**, 1040–1054.e7 (Mar. 2021).

- 765 67. Milner, B. The medial temporal-lobe amnesic syndrome. *Psychiatr Clin North Am*
766 **28**, 599–611, 609 (Sept. 2005).
- 767 68. Eichenbaum, H. The role of the hippocampus in navigation is memory. *J Neuro-*
768 *physiol* **117**, 1785–1796 (Apr. 2017).
- 769 69. Richmond, L. L. & Zacks, J. M. Constructing Experience: Event Models from
770 Perception to Action. *Trends Cogn Sci* **21**, 962–980 (Dec. 2017).
- 771 70. Radvansky, G. A. & Copeland, D. E. Walking through doorways causes forgetting:
772 situation models and experienced space. *Mem Cognit* **34**, 1150–6 (July 2006).
- 773 71. Eichenbaum, H. Is the rodent hippocampus just for 'place'? *Curr Opin Neurobiol*
774 **6**, 187–95 (Apr. 1996).
- 775 72. Zacks, J. M., Kurby, C. A., Eisenberg, M. L. & Haroutunian, N. Prediction error
776 associated with the perceptual segmentation of naturalistic events. *J Cogn Neurosci*
777 **23**, 4057–66 (Dec. 2011).
- 778 73. Carpenter, F., Manson, D., Jeffery, K., Burgess, N. & Barry, C. Grid Cells Form a
779 Global Representation of Connected Environments. *Current Biology* **25**, 1176–1182
780 (2015).
- 781 74. Spiers, H. J., Hayman, R. M. A., Jovalekic, A., Marozzi, E. & Jeffery, K. J. Place
782 field repetition and purely local remapping in a multicompartiment environment.
783 *Cereb Cortex* **25**, 10–25 (Jan. 2015).
- 784 75. Duvelle, É. *et al.* Hippocampal place cells encode global location but not connec-
785 tivity in a complex space. *Curr Biol* **31**, 1221–1233.e9 (Mar. 2021).
- 786 76. Deshmukh, S. S. & Knierim, J. J. Influence of local objects on hippocampal repre-
787 sentations: Landmark vectors and memory. *Hippocampus* **23**, 253–267 (Feb. 2013).
- 788 77. Høydal, Ø. A., Skytøen, E. R., Andersson, S. O., Moser, M.-B. & Moser, E. I.
789 Object-vector coding in the medial entorhinal cortex. *Nature* **568**, 400–404 (Apr.
790 2019).
- 791 78. Low, R. J., Lewallen, S., Aronov, D., Nevers, R. & Tank, D. W. Probing variability
792 in a cognitive map using manifold inference from neural dynamics. *bioRxiv* (2018).
- 793 79. Dudchenko, P. A. & Wood, E. R. in *Space, Time and Memory in the Hippocampal*
794 *Formation* 253–272 (Springer Vienna, 2014).
- 795 80. Kinsky, N. R. *et al.* Trajectory-modulated hippocampal neurons persist throughout
796 memory-guided navigation. *Nature Communications* **11** (May 2020).
- 797 81. Levy, S. J., Kinsky, N. R., Mau, W., Sullivan, D. W. & Hasselmo, M. E. Hippocam-
798 pal spatial memory representations in mice are heterogeneously stable. *Hippocam-*
799 *pus* **31**, 244–260 (Oct. 2020).
- 800 82. Kudrimoti, H., Barnes, C. & McNaughton, B. Reactivation of hippocampal cell
801 assemblies: effects of behavioral state, experience, and EEG dynamics. *J Neurosci*
802 **19**, 4090–101 (May 1999).

- 803 83. Davidson, T. J., Kloosterman, F. & Wilson, M. A. Hippocampal replay of extended
804 experience. *Neuron* **63**, 497–507 (Aug. 2009).
- 805 84. Foster, D. J. & Wilson, M. A. Reverse replay of behavioural sequences in hippocam-
806 pal place cells during the awake state. *Nature* **440**, 680–683 (Mar. 2006).
- 807 85. Karlsson, M. P. & Frank, L. M. Awake replay of remote experiences in the hip-
808 pocampus. *Nature Neuroscience* **12**, 913–918 (June 2009).
- 809 86. Buzsáki, G. Hippocampal sharp wave-ripple: A cognitive biomarker for episodic
810 memory and planning. *Hippocampus* **25**, 1073–188 (Oct. 2015).
- 811 87. Roux, L., Hu, B., Eichler, R., Stark, E. & Buzsáki, G. Sharp wave ripples during
812 learning stabilize the hippocampal spatial map. *Nat Neurosci* **20**, 845–853 (June
813 2017).
- 814 88. Joo, H. R. & Frank, L. M. The hippocampal sharp wave-ripple in memory retrieval
815 for immediate use and consolidation. *Nat Rev Neurosci* **19**, 744–757 (Dec. 2018).
- 816 89. Pfeiffer, B. E. & Foster, D. J. Hippocampal place-cell sequences depict future paths
817 to remembered goals. *Nature* **497**, 74–9 (May 2013).
- 818 90. Ólafsdóttir, H. F., Bush, D. & Barry, C. The Role of Hippocampal Replay in
819 Memory and Planning. *Curr Biol* **28**, R37–R50 (Jan. 2018).
- 820 91. Erdem, U. M. & Hasselmo, M. A goal-directed spatial navigation model using
821 forward trajectory planning based on grid cells. *Eur J Neurosci* **35**, 916–31 (Mar.
822 2012).
- 823 92. Uria, B. *et al.* The Spatial Memory Pipeline: a model of egocentric to allocentric
824 understanding in mammalian brains. *bioRxiv* (2020).
- 825 93. Yoon, K.-J. *et al.* Evidence of low-dimensional continuous attractor dynamics in
826 grid cells. *Nat Neurosci* (In review, 2012).